Low-energy scattering and photoproduction of η mesons on three-body nuclei

A. Fix* and H. Arenhövel
Institut für Kernphysik, Johannes Gutenberg-Universität Mainz, D-55099 Mainz, Germany
(Received 20 February 2003; published 6 October 2003)

The optical potential approach for low-energy scattering of η mesons on three-body nuclei is compared to an exact treatment of the η $3N$ system using four-body scattering theory with separable interactions in s waves only. The higher-order terms including the interaction of the struck nucleon with the surrounding nuclear medium and virtual target excitations in between successive η scatterings are found to cause important corrections. Effects of final state interaction in η photoproduction on ^{3}H and ^{3}He are also studied and sizable contributions beyond the optical model approach are found.

DOI: 10.1103/PhysRevC.68.044002 PACS number(s): 13.60.−r, 13.75.−n, 21.45.+v, 25.20.−x

I. INTRODUCTION

During the last 10 years much effort has been devoted to the study of the interaction of an η-meson with very light nuclei. The attention to this area, called primarily by the pioneering work of Refs. [1,2], arises from the distinctive features of the η-nuclear system at low energies. In more detail we can note the following features.

(i) The ηN interaction is characterized by the $S_{11}(1535)$ resonance located near zero ηN kinetic energy. As a consequence, the s-wave part of the ηN interaction is attractive and rather large near threshold. This considerable attraction which is assumed to be coherently enhanced in nuclei has led to speculations about the existence of η-nuclear bound states which may be formed already in $A=3$ nuclei. Although a calculation using an energy-independent ηA potential has confirmed this hypothesis [2], more sophisticated investigations [3,4] have shown that the ηN interaction is unlikely to yield a bound η $3N$ system even with a relatively large real part of the scattering length Re $a_{\eta N}=0.75$ fm. The pole of the scattering amplitude "recedes" to the nonphysical sheet generating an s-wave virtual state. It is important that apparently the pole is located close to the scattering threshold, resulting in a strong influence on low-energy scattering and production processes with η mesons.

(ii) Concerning the formal aspects, the $S_{11}(1535)$ resonance, dominating the low-energy ηN interaction, must distort the transparent connection between the ηN and ηA scattering amplitudes. This connection is well established in the pion-nuclear case within the local-density limit where the equivalent optical potential is related in a simple fashion to the elementary πN amplitude [5] (except for real absorption of pions on few-nucleon clusters). The physical basis of this fact, giving rise to the so-called impulse approximation of the optical potential, is a large internucleon separation distance compared to the range of the πN interaction. On the contrary, due to the resonance pole in the ηN interaction, the latter must be sizably influenced by the nuclear environment. Indeed, using $\Gamma=75$ MeV for the $S_{11}(1535)$ width near the ηN threshold, we obtain for the collision time $\Delta t=2\hbar/\Gamma \approx 1.7\times10^{-23}$ s which exceeds the time $\Delta t=\hbar/m_\pi \approx 5\times10^{-24}$ s associated with the pion-exchange NN interaction. Therefore, the validity of the simplest optical potential for the ηA interaction is expected to be doubtful, and more rigorous models have to be used.

The purpose of the present paper is to explore the interaction of η mesons with three-body nuclei, a problem which can be solved exactly using methods developed within four-body scattering theory. At the same time, the generalization of the results obtained in this way to heavier nuclei seems to be more justifiable than in the deuteron case, where the two nucleons are strongly kinematically correlated and very weakly bound. Our intention is to analyze the quality of the first-order optical potential for the η $3N$ interaction using as a reference the exact four-body calculation. Since we have no way of direct fitting η-nuclear scattering cross sections using a phenomenological potential model, the information on the low-energy η-nuclear interaction stems entirely from the assumed properties of the ηN interaction and depends strongly on the model linking these two processes. For this reason, a thorough microscopic approach to the η-nuclear dynamics becomes particularly important. On the other hand, rather complex mathematical infrastructure of the four-body scattering theory prevents to some extent a simple interpretation of the results. Therefore, we first will clarify the question, whether the η-nuclear interaction can be adequately described in terms of an optical potential. Furthermore, the comparison of the four-body results with those obtained using less rigorous but very tractable approaches, such as the lowest-order optical potential, may be very fruitful in understanding the η $3N$ interaction mechanism.

There exists already a variety of studies with respect to the validity of the optical model approach by comparing the corresponding results with the ones provided by the few-body scattering equations. In particular, higher-order contributions to the pion- or nucleon-deuteron optical potential were analyzed in Refs. [6–8]. However, because of the distinctive properties of ηN low-energy interaction mentioned above we find it necessary to examine the applicability of the optical model to the ηA scattering as a topic of its own right.

Several aspects concerning the accuracy of the simplest optical model for the scattering of η mesons on s-shell nuclei

*On leave from Tomsk Polytechnic University, 634034 Tomsk, Russia.

were already discussed in Ref. [3]. In particular, it was shown that the behavior of the ηN scattering matrix below the free threshold has a crucial influence on the results. Here we address other questions related to the optical potential approach for $\eta\,3N$ scattering, which as follows.

(i) What is the influence of binding of the participating nucleon on the elementary scattering process?

(ii) What is the relative importance of target excitations in between two successive scatterings on different nucleons?

(iii) What is the importance of the short-range behavior of the nucleon-nucleon potential?

The second part of the paper is devoted to coherent η photoproduction on three-body nuclei

$$\gamma + {}^3\mathrm{H}/{}^3\mathrm{He} \rightarrow \eta + {}^3\mathrm{H}/{}^3\mathrm{He}. \tag{1}$$

These reactions are of special importance in η-nuclear physics. First, the main driving mechanism of η photoproduction, the photoexcitation of the $S_{11}(1535)$-resonance, is well established. This is in contrast to reactions with nucleons as incident particles, where the main mechanism connected with the short-range part of the NN interaction is presumably much more complex and as of yet not well understood. Second, the energy gap between the coherent and incoherent thresholds, where the η yield is free from the strong incoherent background is about $\Delta E_\gamma = 7$ MeV, which is appreciably larger than the one on the deuteron (about 3 MeV). This advantage has been partially used in a recent $^3\mathrm{He}(\gamma,\eta)^3\mathrm{He}$ experiment carried out with the TAPS facility operating at MAMI [9]. Third, the η-nuclear interaction, which is most important in the s wave, must be particularly significant in reactions involving nuclei with nonzero spin. As a counter example, the reaction $^4\mathrm{He}(\gamma,\eta)^4\mathrm{He}$, where the s wave in the final state is totally suppressed, does not show any strong influence of the final state interaction (FSI). Finally, the dynamics of reactions (1) may be treated within a few-body scattering theory, i.e., formally exactly. Though the near-threshold η photoproduction on three-body nuclei was already considered in Ref. [10] within the so-called finite-rank approximation (FRA), we reexamine it primarily in order to show the results of the four-body approach for the $\eta\,3N$ interaction in the final state.

The outline of the paper is as follows. First, we briefly review in Sec. II the four-body formalism which is relevant for the present consideration. For the separable representation of the kernels we use the energy-dependent pole expansion method of Ref. [11]. In Sec. III, after a short summary of the Kerman-McManus-Thaler theory, we discuss the "standard" optical model for the $\eta\,3N$ elastic scattering with particular emphasis on the role of the higher-order corrections such as nucleon-core interaction and virtual target excitations. The η photoproduction on three-body nuclei is presented in Sec. IV where we illustrate the strong effect of the $\eta\,3N$ interaction in the final state. In this section we also compare our predictions with those given in Ref. [10]. The main results are reviewed in the conclusion.

II. THE FOUR-BODY APPROACH TO $\eta\,3N$ SCATTERING

We begin the formal part with a brief review of the four-body scattering formalism applied to $\eta\,3N$ scattering. Our basic tool for solving the four-body equations is the quasiparticle method, reduced to a purely separable representation for the driving two-body potentials and also for the subamplitudes in the (3+1) and (2+2) partitions. The main features of the method were widely presented in the literature (see, e.g., Ref. [12], and references therein). In applying this approach to the $\eta\,3N$ problem, the relevant formalism is considered in Ref. [4]. Within the quasiparticle method, the whole dynamics is described in terms of the amplitudes $X_{\alpha 1}$ $(\alpha=1,2,3)$ connecting the three quasi-two-body channels characterized by the following partitions:

$$\alpha=1{:}\,\eta+(3N),\quad \alpha=2{:}N+(\eta NN),\quad \alpha=3{:}(\eta N)+(NN) \tag{2}$$

with the initial channel $\alpha=1$. To be specific, we consider the triton as target. Because we neglect Coulomb forces and thus isospin invariance holds, the channels with ^{3}H and ^{3}He are identical. Since only the energies up to the three-body threshold will be considered, we treat the pion energy relativistically but use nonrelativistic kinematics for nucleons and the η meson. Furthermore, due to strong dominance of s waves in NN and ηN scattering, we assume that in the low-energy region only the lowest partial wave $(L=0)$ in the $\eta\,3N$ system has to be taken into account.

The essence of the calculational scheme is the solution of the scattering problem for the two- and three-body subsystems specified in partitions (2). For $\alpha=1$ and 2 we deal with interacting three-body systems. Using separable representations for the NN and ηN potentials, the corresponding scattering amplitudes can be expressed in terms of effective quasi-two-body amplitudes $U_{\alpha;ij}(q,q';\mathcal{E})$, which describe the scattering of a particle on a two-body cluster (quasiparticle). The corresponding states are specified by the indices i,j marking the quasiparticles, e.g., $i,j\in\{d,N^*\}$ for $\alpha=2$, where the (NN) and (ηN) systems are denoted as d and N^*, respectively. The notation N^* is associated with the $S_{11}(1535)$ resonance which dominates the low-energy ηN interaction. For $\alpha=3$ we have two independent two-particle subsystems. The relevant amplitudes are also represented in the quasi-two-body form $U_{3;ij}(q,q';\mathcal{E})$ with $i,j\in\{d,N^*\}$ [4].

The reduction of the four-body equations to a numerically manageable form is achieved by expanding the amplitudes $U_{\alpha;ij}$ into separable series of finite rank N_α,

$$U^{(ss')}_{1;dd}(q,q';\mathcal{E}) = \sum_{l,m=1}^{N_1} v^{1(s)}_{d;l}(q;\mathcal{E})\Theta_{1;lm}(\mathcal{E})v^{1(s')}_{d;m}(q';\mathcal{E}), \tag{3}$$

$$U^{(s)}_{\alpha;ij}(q,q';\mathcal{E}) = \sum_{l,m=1}^{N_\alpha} v^{\alpha(s)}_{i;l}(q;\mathcal{E})\Theta^{(s)}_{\alpha;lm}(\mathcal{E})v^{\alpha(s)}_{j;m}(q';\mathcal{E}),\quad \alpha=2,3. \tag{4}$$

To condense the formulas to follow, we use here a unified notation for the vertex functions or form factors v^α in all

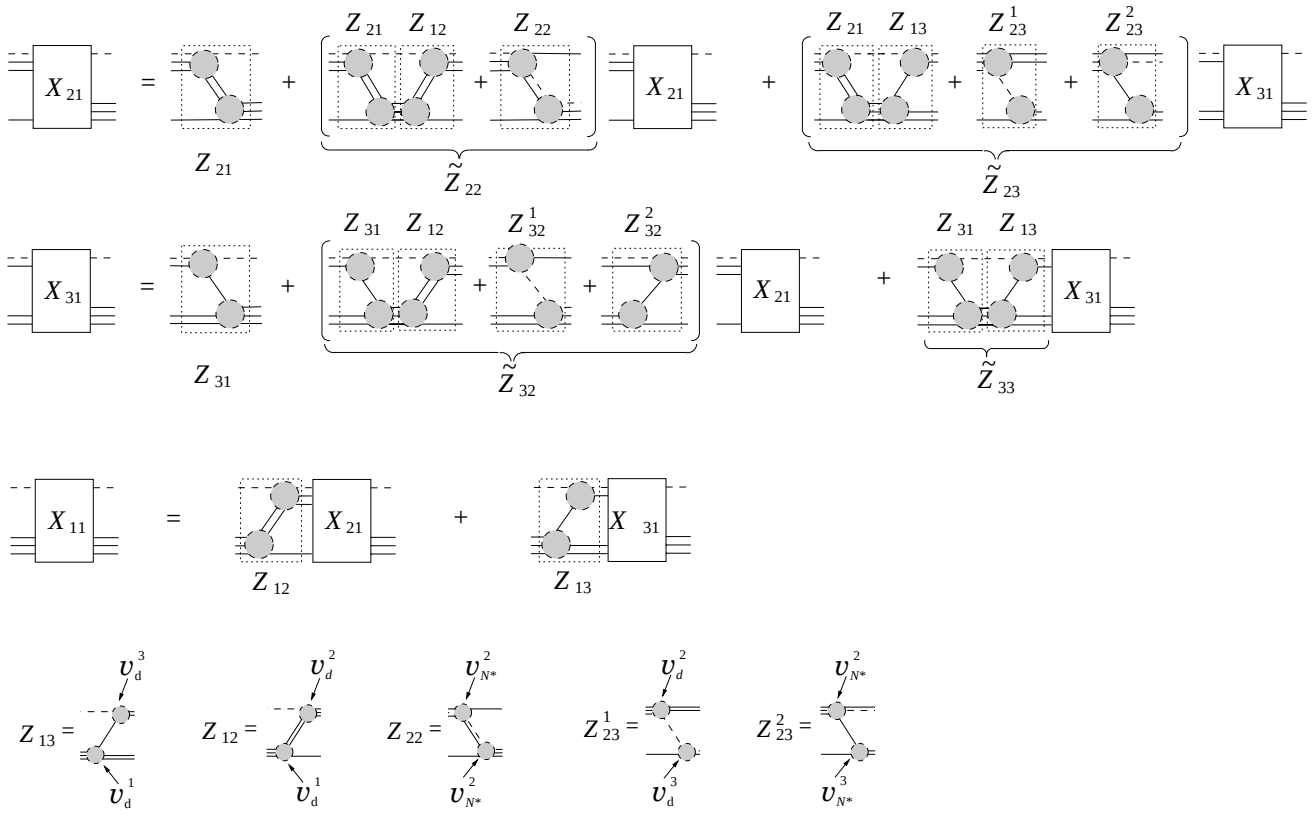

FIG. 1. Diagrammatic representation of the coupled integral Eqs. (5) and (9) for the $\eta\,3N$ scattering and the effective potentials $Z_{\alpha\beta}$ and $\widetilde{Z}_{\alpha\beta}$. The dashed line represents an η meson. The lines close together indicate different two- and three-body quasiparticles.

three channels. They are related to the ones introduced in Ref. [4] as $v^1_{d;n}=u_n, v^2_{i;n}=v_{i;n}, v^3_{i;n}=w_{i;n}$, $i\in\{d,N^*\}$. For the sake of clarity, we note that the amplitude U_1 of the $(NN)+N$ scattering is a 2×2 matrix according to the spin index $s=0,1$ (we need only spin-doublet $3N$ states). Here the values $s=0,1$ denote the total spin of the (NN) s-wave cluster with isospin $t=1-s$. At the same time, in the partitions $\alpha=2,3$, we have two one-dimensional amplitudes $U^{(s)}_\alpha$. For instance, in the channel $\alpha=2$ the index s numerates two independent ηNN states with $J^\pi=0^-$ $(s=0)$ and $J^\pi=1^-$ $(s=1)$, respectively.

Considering the identity of the nucleons, the $\eta\,3N$ problem is reduced to a 3×3 set of integral equations in one scalar variable. For the transition amplitudes $X_{\alpha1}$ connecting the channel 1 to the channels $\alpha=2$ and 3 we arrive at a coupled set of equations

$$X^{(ss')}_{\alpha1;nn'}(p,p';E)=Z^{(ss')}_{\alpha1;nn'}(p,p';E)+\sum_{\beta=2,3}\sum_{l,m}\sum_{\sigma=0,1}\int_0^\infty \widetilde{Z}^{(s\sigma)}_{\alpha\beta;nl}\times(p,p'';E)\,\Theta^{(\sigma)}_{\beta;lm}\left(E-\frac{p''^2}{2M_\beta}\right)X^{(\sigma s')}_{\beta1;mn'}\times(p'',p';E)\,\frac{p''^2\,dp}{2\pi^2},\quad \alpha=2,3, \tag{5}$$

where $Z_{\alpha\beta}$ and $\widetilde{Z}_{\alpha\beta}$ are the effective potentials realized through particle exchange between the quasiparticles in the channels α and β. The arguments of the effective propagators Θ_α are the internal energies of the corresponding clusters, given in Eq. (2). In the case $\alpha=3$ it is equal to the sum of the c.m. kinetic energies in the ηN and NN subsystems. The reduced masses in the three channels read

$$M_1=\frac{3M_Nm_\eta}{3M_N+m_\eta},\quad M_2=\frac{M_N(2M_N+m_\eta)}{3M_N+m_\eta},\quad M_3=\frac{2M_N(M_N+m_\eta)}{3M_N+m_\eta}. \tag{6}$$

Equations (5) are illustrated in Fig. 1, where also the structure of the potentials $Z_{\alpha\beta}$ and $\widetilde{Z}_{\alpha\beta}$ is schematically explained. The former are expressed in terms of the form factors $v^\alpha_{i;n}$ as

$$Z^{(ss')}_{\alpha\beta;nn'}(p,p';E)=\frac{\Omega_{ss'}}{2}\sum_j\int_{-1}^{+1}v^{\alpha(s)}_{j;n}\left(q,E-\frac{p^2}{2M_\alpha}\right)\tau^{(s)}_j\times\left(E-\frac{p^2}{2M_\alpha}-\frac{q^2}{2\mu^\alpha_j}\right)v^{\beta(s')}_{j;n'}\times\left(q',E-\frac{p'^2}{2M_\beta}\right)d(\hat p\cdot\hat p'). \tag{7}$$

Here, the functions $\tau_j(z)$ are the familiar quasiparticle

propagators appearing in the separable model for $NN(j=d)$ and $\eta N(j=N^*)$ scattering which depend on the two-body c.m. kinetic energies. The corresponding reduced masses μ_j^α read

$$\mu_d^1=\frac{3}{2}M_N,\quad \mu_d^2=\frac{2M_Nm_\eta}{2M_N+m_\eta},\quad \mu_{N^*}^2=\frac{M_N(M_N+m_\eta)}{2M_N+m_\eta},$$

$$\mu_d^3=\frac{M_Nm_\eta}{M_N+m_\eta},\quad \mu_{N^*}^3=\frac{M_N}{2}. \tag{8}$$

The spin-isospin coefficients are denoted by $\Omega_{ss'}$. Clearly, due to the pseudoscalar-isoscalar nature of the η meson the spin s of the NN cluster fixes uniquely the order of the spin-isospin coupling of the whole $\eta\,3N$ configuration. The momenta q and q' in Eq. (7) are functions of the variables $\vec{p},\vec{p}'$, and E as given in Ref. [4]. The overall c.m. energy E is counted from the four-body threshold, i.e., $E=W-3M_N-m_\eta$ with W being the η^3H invariant mass. Below the first inelastic threshold the obvious relation $E\leqslant-\varepsilon_d$ holds, where ε_d denotes the deuteron binding energy. For more details concerning the structure of the potentials $\widetilde{Z}_{\alpha\beta}$ and $Z_{\alpha\beta}$ we refer to Ref. [4].

Elastic η^3H scattering is described by the amplitude X_{11}, which is determined by the amplitudes $X_{\alpha1}$ $(\alpha=2,3)$ as

$$X^{(ss')}_{11;nn'}(p,p';E)=\sum_{\alpha=2,3}\sum_{l,m}\sum_{\sigma=0,1}\int_0^\infty Z^{(s\sigma)}_{1\alpha;nl}(p,p'';E)\;\Theta^{(\sigma)}_{\alpha;lm}\times\left(E-\frac{p''^2}{2M_\beta}\right)X^{(\sigma s')}_{\alpha1;mn'}(p'',p';E)\;\frac{p''^2dp}{2\pi^2}. \tag{9}$$

As was already mentioned, the key point of the reduction procedure, leading to numerically manageable equations (5), is the separable expansion of subamplitudes (3) and (4). In the present paper we use for this purpose the method of the energy-dependent pole expansion (EDPE), presented in detail in Ref. [11]. The starting point is the eigenvalue equation for the vertex functions $v^\alpha_{i;n}(q,\mathcal{E})$,

$$v^{1(s)}_{d;n}(q,B_1)=\frac{1}{\lambda^1_n}\sum_{s'=0,1}\int_0^\infty V^{(ss')}_{1;dd}(q,q';B_1)\;\tau_d^{(s')}\left(B_1-\frac{q'^2}{2\mu_d^1}\right)v^{1(s')}_{d;n}(q',B_1)\frac{q'^2dq'}{2\pi^2}, \tag{10}$$

$$v^{\alpha(s)}_{i;n}(q,B_\alpha)=\frac{1}{\lambda^{\alpha(s)}_n}\sum_{j=d,N^*}\int_0^\infty V^{(s)}_{\alpha;ij}(q,q';B_\alpha)\;\tau_j^{(s)}\left(B_\alpha-\frac{q'^2}{2\mu_j^\alpha}\right)v^{\alpha(s)}_{j;n}(q',B_\alpha)\frac{q'^2dq'}{2\pi^2},\quad \alpha=2,3. \tag{11}$$

The explicit expressions for the effective potentials $V_{\alpha;ij}(q,q';\mathcal{E})$ are given in Ref. [4]. Equations (10) are solved for an arbitrarily fixed energy $\mathcal{E}=B_\alpha$. In the actual calculation we have taken $B_1=-\varepsilon_{^3\mathrm{H}}$ (the triton binding energy) and $B_\alpha=-\varepsilon_d$ in the other two channels $\alpha=2,3$.

The extrapolation of the vertices $v^\alpha_{i;n}$ onto the whole energy axes is carried out according to the expressions

$$v^{1(s)}_{d;n}(q,\mathcal{E})=\sum_{s'=0,1}\int_0^\infty V^{(ss')}_{1;dd}(q,q';\mathcal{E})\;\tau_d^{(s')}\left(B_1-\frac{q'^2}{2\mu_d^1}\right)\times v^{(s')}_{d;n}(q',B_1)\frac{q'^2dq'}{2\pi^2}, \tag{12}$$

$$v^{\alpha(s)}_{i;n}(q,\mathcal{E})=\sum_{j=d,N^*}\int_0^\infty V^{(s)}_{\alpha;ij}(q,q';\mathcal{E})\;\tau_j^{(s)}\left(B_\alpha-\frac{q'^2}{2\mu_j^\alpha}\right)\times v^{\alpha(s)}_{j;n}(q',B_\alpha)\frac{q'^2dq'}{2\pi^2},\quad \alpha=2,3. \tag{13}$$

The effective EDPE propagators Θ_α in Eqs. (3) and (4) are defined by

$$[\Theta_1^{-1}(\mathcal{E})]_{mn}=\sum_{s=0,1}\int_0^\infty\left[v^{1(s)}_{d;m}(q,B_1)\tau_d^{(s)}\left(B_1-\frac{q^2}{2\mu_d^1}\right)-v^{1(s)}_{d;m}\times(q,\mathcal{E})\tau_d^{(s)}\left(\mathcal{E}-\frac{q^2}{2\mu_d^1}\right)\right]v^{1(s)}_{d;n}(q,\mathcal{E})\frac{q^2dq}{2\pi^2}, \tag{14}$$

$$[\Theta_\alpha^{(s)-1}(\mathcal{E})]_{mn}=\sum_{j=d,N^*}\int_0^\infty\left[v^{\alpha(s)}_{j;m}(q,B_\alpha)\tau_j^{(s)}\left(B_\alpha-\frac{q^2}{2\mu_j^\alpha}\right)-v^{\alpha(s)}_{j;m}(q,\mathcal{E})\tau_j^{(s)}\left(\mathcal{E}-\frac{q^2}{2\mu_j^\alpha}\right)\right]v^{\alpha(s)}_{j;n}\times(q,\mathcal{E})\frac{q^2dq}{2\pi^2},\quad \alpha=2,3. \tag{15}$$

In the calculation, we use a 6×6 separable representation (3) and (4) in each partition (2) which yields accurate solutions up to the first inelastic threshold.

Due to the strong coupling between the ηN and πN channels in the $S_{11}(1535)$ region, the transitions $\eta N\leftrightarrow\pi N$ must in general be taken into account. Clearly, the most straightforward way to introduce the pion degrees of freedom would be to generalize the $\eta\,3N$ four-body equations to include the coupled channels $(\pi\,3N)\leftrightarrow(\eta\,3N)$. But in practice, the four-body treatment of the $\pi\,3N$ states turns out to be very complicated. The reason for this is the appearance of moving singularities arising near the physical region for the πNN amplitudes above the three-body threshold. As a result, the separable representation of the four-body kernels converges very poorly [13]. Therefore, we neglect the channel $\pi\,3N$ keeping only the intermediate πN "bubbles" in the $S_{11}(1535)$ propagator. The validity of this neglect seems to be doubtful, since the πN interaction in the second resonance region is visibly stronger than the ηN one. The crucial point, however, is that the two-step process $\eta N\rightarrow\pi N\rightarrow\eta N$, favoring large momenta of the intermediate pion $k_\pi\approx400$ MeV/c, needs two nucleons to be within the range $R=\hbar/k_\pi\approx0.5$ fm. Adopting a simple geometric interpretation, the corresponding mechanism is associated with a small probability

$$P = \frac{4}{3}\pi R^3 \, \rho_{^3\mathrm{H}}(0) \approx \frac{1}{10}, \tag{16}$$

where $\rho_{^3\mathrm{H}}(r)$ is the ^{3}H nucleon density, and thus is not expected to be effective for low-energy η^3H scattering.

For the target wave function we take only the *s*-wave part

$$\Psi_{M_J M_T}(\vec{q}, \vec{k}) = \frac{1}{\sqrt{3}}(1 - P_{12} - P_{13}) \sum_{s=0,1} \psi^{(s)}(q_1, k_{23}) \times \left[\left[\frac{1}{2} \times \frac{1}{2} \right]^{st} \times \frac{1}{2} \right]^{(1/2)M_J (1/2)M_T}, \tag{17}$$

where the isospin $t=1-s$ and M_J and M_T denote total spin and isospin projections, respectively. The spatial functions $\psi^{(s)}(q_1, k_{23})$ are taken symmetric with respect to the nucleons 2 and 3. They are extracted from the bound state pole of the $3N$ scattering amplitude, calculated within the three-body model. The corresponding expression in terms of the $(3N) \to N + (NN)$ vertices $v^{1(s)}_{d;1}$ reads

$$\psi^{(s)}(q, k) = -N g^{(s)}_d \tau^{(s)}_d \left(-\varepsilon_{^3\mathrm{H}} - \frac{3q^2}{4M_N} \right) \frac{v^{1(s)}_{d;1}(q, -\varepsilon_{^3\mathrm{H}})}{\varepsilon_{\mathrm{H}} + \frac{3q^2}{4M_N} + \frac{k^2}{M_N}}. \tag{18}$$

The normalization factor is obtained from the residue of the scattering matrix

$$N^{-2} = \left. \frac{d\lambda^1_1}{d\mathcal{E}} \right|_{\mathcal{E} = -\varepsilon_{^3\mathrm{H}}}, \tag{19}$$

where λ^1_1 is the first eigenvalue of the kernel $V_{1;dd}\tau_d$ [see Eq. (10)]. Finally, for the η^3H scattering amplitude we get

$$F_{\eta^3\mathrm{H}}(k_\eta) = -\frac{\mu_{\eta^3\mathrm{H}}}{2\pi} \sum_{s,s'=0,1} X^{(ss')}_{11;11}(k_\eta, k_\eta; E), \tag{20}$$

with the η^3H reduced mass $\mu_{\eta^3\mathrm{H}}$ and the on-shell momentum $k_\eta = [2\mu_{\eta^3\mathrm{H}}(E + \varepsilon_{^3\mathrm{H}})]^{1/2}$.

As was already noted, we consider the NN and ηN interactions only in *s* states. For the NN $^1S_0$ and $^3S_1$ configurations we adopt a rank-1 separable parametrization

$$v^{(s)}_{NN}(k, k') = -g^{(s)}_d(k) g^{(s)}_d(k'), \quad \text{with } g^{(s)}_d(k) = \sqrt{2}\pi \sum_{i=1}^{6} \frac{C^{(s)}_i}{k^2 + \beta^{(s)2}_i} \quad \text{for } s = 0, 1, \tag{21}$$

where the parameters $C^{(s)}_i$ and $\beta^{(s)}_i$ are listed in Ref. [14]. The index $s=0,1$ refers to the singlet and triplet states, respectively. The separable potential (21) is obtained by fitting the off-shell behavior of the Paris NN potential at zero energy and is therefore appropriate for processes without target breakup. The corresponding three-body calculation gives for the triton binding energy a reasonable value $\varepsilon_{^3\mathrm{H}} = 8.64$ MeV and describes rather well the ^{3}H charge form factor up to $Q^2 = 8$ fm^{-2}.

As for the ηN interaction, we use here the simplest separable parametrization with the energy-dependent potential

$$v_{\eta N}(k, k'; W) = \frac{g^{(\eta)}_{N^*}(k) g^{(\eta)}_{N^*}(k')}{W - M_0}, \quad \text{with } g^{(\eta)}_{N^*}(k) = \frac{g^{(\eta)}_{N^*}}{\sqrt{2\omega_\eta}} \frac{\beta^{(\eta)2}_{N^*}}{k^2 + \beta^{(\eta)2}_{N^*}}, \tag{22}$$

which gives the familiar isobar ansatz for the meson-nucleon amplitude with the bare resonance mass M_0. In the present paper, the excitation of the $S_{11}(1535)$ resonance is assumed to be the only mechanism for the meson-nucleon interaction. Rather than to investigate the dependence of the results on the ηN scattering length $a_{\eta N}$, we preferred to choose the parameters in Eq. (22) such that the ηN scattering length

$$a_{\eta N} = (0.50 + i0.32)\,\mathrm{fm} \tag{23}$$

is reproduced. This value lies approximately "halfway" in the listing of various ηN scattering lengths which can be found in the literature (see, e.g., Ref. [15]). It must be noted that the low-energy η-nuclear interaction depends strongly on the continuation of the ηN amplitude to negative kinetic energies and hence must be sensitive to the amplitudes in the channels coupled to the ηN one. Therefore, we use here the unitary model of Ref. [16] where three coupled channels $\eta N, \pi N$, and $\pi\pi N$ are considered. In order to reproduce value (23) we have slightly changed the set of parameters presented in Ref. [16] in such a manner that the $\pi N \to \pi N$ and $\pi N \to \eta N$ scattering data are reasonably well described in the region below and just above the ηN threshold. The results shown in Fig. 2 are obtained with the parameter values

$$g^{(\pi)}_{N^*} = 8.898/\sqrt{12\pi}, \quad \beta^{(\pi)}_{N^*} = 404 \text{ MeV}, \qquad g^{(\eta)}_{N^*} = 7.090/\sqrt{4\pi}, \quad \beta^{(\eta)}_{N^*} = 695 \text{ MeV}, \qquad M_0 = 1599 \text{ MeV}. \tag{24}$$

The additional factors in Eq. (24) appear due to different normalizations of the meson-nucleon potentials $v_{\pi N}$ and $v_{\eta N}$ used in this work and in Ref. [16]. The parameters of the two-pion channel $\pi\pi N$ were taken unchanged from Ref. [16].

III. THE OPTICAL MODEL FOR η^3H SCATTERING

We begin the analysis of the optical potential approach by reviewing the corresponding formalism. According to the Watson multiple scattering theory [19], the η-nuclear interaction may be treated as a series of ηN collisions. In the present discussion we use the version put forward by Kerman-McManus-Thaler (KMT) [20]. The corresponding expansion of the scattering operator reads

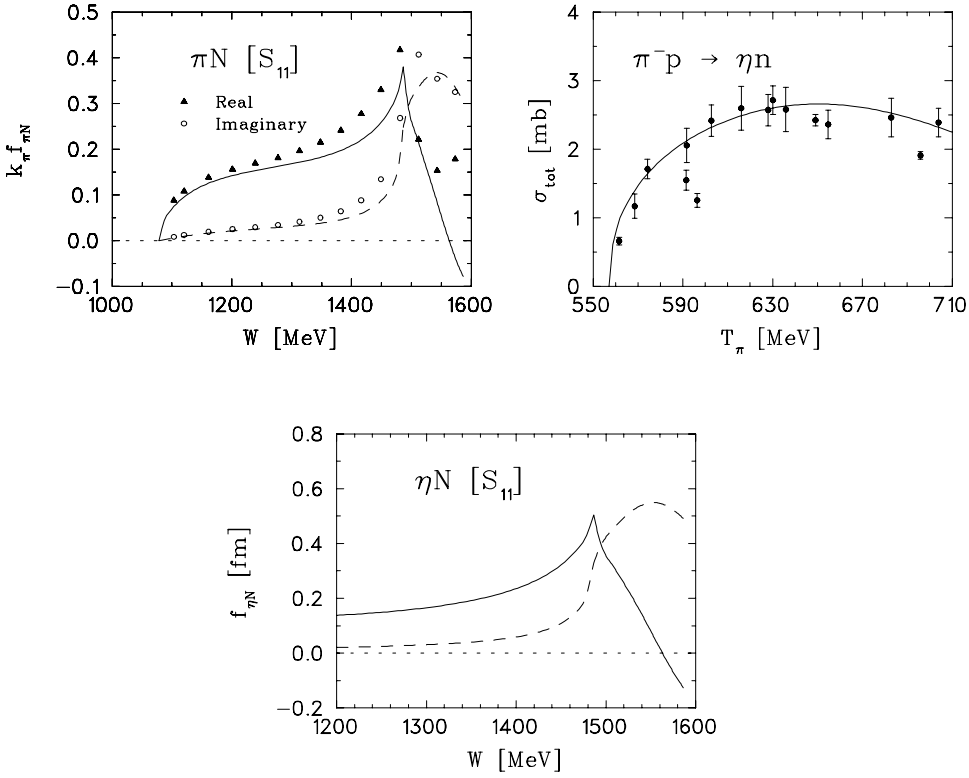

FIG. 2. Upper left panel: the S_{11} partial wave of the πN scattering amplitude predicted by the parametrization of $S_{11}(1535)$ resonance used in the present paper [see Eqs. (22) and (24)]. Notations: solid curve—real part, dashed—imaginary part. Circles and triangles represent the result of the VPI analysis [17]. Upper right panel: total $\pi^- p \to \eta n$ cross section. The data are taken from the compilation presented in Ref. [18]. Lower panel: the ηN off-shell scattering amplitude at $q = q' = 0$. Notations as in the upper left panel.

$$T = \sum_{i}^{A} \tau(i) + \sum_{i \neq j}^{A} \tau(i) G \, \tau(j) + \cdots . \tag{25}$$

Here Green's function G describes the propagation of a free η and A interacting nucleons

$$G = \frac{\hat{A}}{E - H_0 - V_A}, \tag{26}$$

where the nuclear potential V_A describes the interactions of the nucleons, and the free Hamiltonian H_0 includes only the kinetic energy operator of meson and nucleons. Furthermore, we have included into Green's function the projection operator $\hat{A}$ onto the completely antisymmetric nuclear states. The scattering matrix τ in Eq. (25) describes the off-shell scattering of an η meson on a single bound nucleon and obeys the equation

$$\tau = v_{\eta N} + v_{\eta N} G \, \tau. \tag{27}$$

Within the KMT theory the nucleons are treated to be identical from the beginning. Therefore we have dropped the nucleon index i in Eq. (27).

The operator U of the equivalent optical potential is usually introduced by rewriting Eq. (25) in the form

$$T = U + \frac{A-1}{A} \, U G P_0 T, \tag{28}$$

where P_0 is the projector onto the nuclear ground state. The many-body aspects of the problem are then incorporated in the operator U which obeys the equation

$$U = U^{(1)} + \frac{A-1}{A} \, U^{(1)} G (1 - P_0) U, \tag{29}$$

with the driving term $U^{(1)} = A\tau$.

In the present paper we explore two approximations to the potential U which have been used in previous work in low-energy η-nuclear physics.

(i) Coherent approximation: here one keeps only the leading term in Eq. (29). The resulting optical potential is given by the ground state expectation value of the matrix τ times the number of nucleons in the nucleus

$$U_C(\vec{p}, \vec{p}\,'; E) = \langle 0; \vec{p} | U^{(1)}(E) | 0; \vec{p}\,' \rangle = A \langle 0; \vec{p} | \tau | 0; \vec{p}\,' \rangle . \tag{30}$$

As may be seen, the restriction to the first-order term $U^{(1)}$ in expansion (29) neglects the virtual target excitations in between successive scatterings on different nucleons. Of course, as follows from Eq. (27), excitations are allowed when η interacts successively with the same nucleon. One of the points in favor of the coherent approximation is the assumed dominance of the nearest singularity (bound state pole). Probably no less important is the orthogonality of the nuclear ground state wave function to the excited states, which results in a reduction of the matrix element $\langle 0 | U^{(1)} | n \rangle$ at least at small momentum transfers. However, in spite of these reasonable arguments the study of nd [21] and ηd [22] scattering has shown that keeping only the target ground state weakens sizably the overall interaction in the system and is therefore a rather poor approximation.

(ii) Impulse approximation: it is considered as a further simplification of the approximation (i) and consists of the

substitution of the operator τ in Eq. (30) by the free-space ηN scattering matrix $t_{\eta N}$ satisfying the equation

$$t_{\eta N} = v_{\eta N} + v_{\eta N} G_0 t_{\eta N}, \quad \text{with } G_0 = \frac{1}{E - H_0}. \tag{31}$$

The resulting optical potential for the η^3H scattering is then

$$\begin{aligned} U_I(\vec{p}, \vec{p}\,'; E) &= A\langle 0; \vec{p}|t_{\eta N}|0; \vec{p}\,'\rangle \\ &= A \int \Psi^*_{^3\mathrm{H}}(\vec{q}, \vec{k}) t_{\eta N}(w_{\eta N}(\vec{q}))\Psi_{^3\mathrm{H}} \\ &\quad \times \left(\vec{q} + \frac{2}{3}(\vec{p} - \vec{p}\,'), \vec{k}\right) \frac{d^3q}{(2\pi)^3} \frac{d^3k}{(2\pi)^3}, \end{aligned} \tag{32}$$

where the argument $\vec{q}$ of the ground state wave function $\Psi_{^3\mathrm{H}}$ is the relative momentum of the participating nucleon with respect to the other two nucleons. Thus within this approximation, the struck nucleon is bound only before and after the interaction with the incident meson but is free during the scattering. The role of the surrounding nucleons is to provide only the momentum distribution for the active scatterer. The impulse approximation is more or less successful for low-energy pion-nucleus scattering far away from the resonance region [5], that is, for light projectiles which interact weakly with the target constituents. But its validity may be marginal in the η-nuclear case. The main reason for this fact is that the impulse approximation breaks down if the projectile is in resonance with the nucleon [19]. As was already noted in the Introduction, since the ηN scattering is associated with a nonvanishing time delay due to the $S_{11}(1535)$ resonance, the interaction of the struck nucleon with the remaining ones must be generally important.

In order to study the quality of approximations (i) and (ii) for the η-nuclear interaction we have calculated the η^3H elastic scattering using the optical potentials U_C (30) and U_I (32). In each case only the *s*-wave part of the scattering amplitude was taken into account. The results are obtained by solving Eq. (28) in momentum space

$$\begin{aligned} T(p, p; E) &= U(p, p; E) \\ &\quad + \frac{2}{3} \frac{\mu_{\eta^3\mathrm{H}}}{\pi^2} \int_0^\infty \frac{U(p, p'; E) T(p', p; E)}{p^2 - p'^2 + i\varepsilon} p'^2 dp'. \end{aligned} \tag{33}$$

The numerical difficulties caused by the singularity in the integrand at $p' = p$ were eliminated with the help of the Noyes-Kowalski trick [23].

It is worthwhile to note that since the in-medium ηN scattering matrix τ is an $(A+1)$-body operator, its full treatment is in general possible only with certain approximations. However, in the case of $A=3$, Eq. (27) can be solved exactly using the four-body formalism. Indeed, this equation represents the reduced problem where the η meson is scattered off only one of the nucleons which in turn interacts with the other two nucleons. Therefore, using the separable representation for the two- and three-body scattering matrices as described in Sec. II, Eq. (27) can be transformed into the form

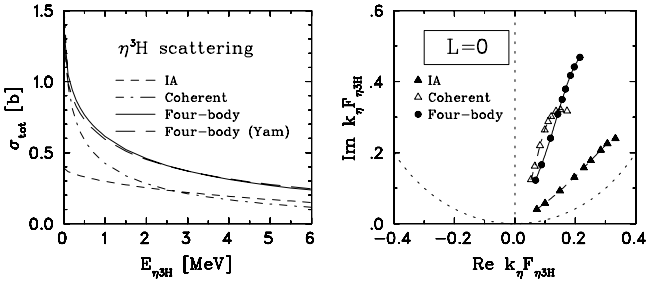

FIG. 3. Elastic cross section for η^3H scattering (left panel) and Argand plot (right panel) of the scattering amplitude. The dashed curves (filled triangles on the right panel) represent the impulse approximation to the first-order optical potential [Eq. (32)]. In the dash-dotted curves (open triangles) the medium corrections to the single scattering are taken into account [Eq. (30)]. The solid curves (filled circles) represent the result of the full four-body calculation. The long-dashed curve in the left panel is obtained with the Yamaguchi *NN* potential embedded into the nuclear sector. In the right panel the circles and triangles indicate the following c.m. kinetic energies: $E_{\eta^3\mathrm{H}}$=0.1,0.2,0.5,1.0,1.5,2.0,3.0,4.0, and 6.0 MeV.

presented in Eqs. (5) and (9) where now we must switch off the η exchange between the nucleons. In the computation, we simply set the potential $V_{2;N^*N^*}$ in Eqs. (11) and (13) as well as the term $Z^1_{23}(Z^1_{32})$ in the potential $\widetilde{Z}_{23}(\widetilde{Z}_{32})$ (see Fig. 1) equal to zero. The matrix X_{11}, obtained in this way, yields the *s*-wave potential U_C (30) for the η^3H scattering in the form

$$U_C(p, p'; E) = \sum_{ss'=0,1} X^{(ss')}_{11;11}(p, p'; E). \tag{34}$$

In Fig. 3 we compare the results of approximations (30) and (32) with those given by the four-body theory where the $\eta\,3N$ multiple scattering series (25) is summed exactly. There are two main conclusions to be drawn from this comparison.

(i) The η^3H interaction generated by the optical potential U_I (32) is relatively weak. It is interesting to compare our result with that obtained within the scattering length approximation $t_{\eta N} \to -(2\pi/\mu_{\eta N}) a_{\eta N}$. The latter predicts a binding of the $\eta\,3N$ system already for relatively modest values of $a_{\eta N}$ (see, e.g., Refs. [2,24]). The trivial source of this discrepancy lies in the strong energy dependence of the ηN amplitude which is ignored by the scattering length approximation. The change of the free ηN energy $w^{\mathrm{free}}_{\eta N}$ in the medium is primarily due to the Fermi motion and due to the binding of the nucleons. A rough estimation at zero η^3H kinetic energy gives

$$\Delta\omega = w_{\eta N} - w^{\mathrm{free}}_{\eta N} \approx -\varepsilon_b - \frac{\langle q^2\rangle}{2M_3}, \tag{35}$$

where $\varepsilon_b \approx 6.5$ MeV is the binding energy of a participating nucleon to the two-nucleon core, while $\langle q^2\rangle$ stands for the mean squared nucleon momentum inside the nucleus, and the reduced mass M_3 is given by Eq. (6). Taking $\sqrt{\langle q^2\rangle} = 120$ MeV/c we obtain $\Delta\omega \approx -15$ MeV. In the calculation, the energy at which the ηN amplitude has to be calculated was chosen according to the so-called "specta-

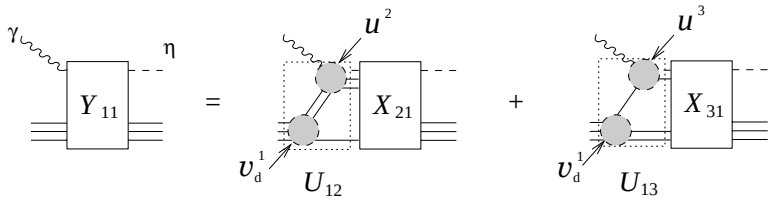

FIG. 4. The photon-induced effective potentials appearing in leading order of the electromagnetic interaction in η photoproduction on three-body nuclei (37).

tor on-shell" prescription. The corresponding energy shift $|\Delta\omega|$ is larger than that given by estimation (35) where the internal energy of the two-nucleon core is neglected. Taking into account the difference $\Delta\omega$ results in decreasing the ηN scattering amplitude and especially its imaginary part, which has a sharp energy dependence around the ηN threshold (see Fig. 2). The crucial importance of this fact was also discussed in Refs. [3,15]. One sees in Fig. 3 that inclusion of the intermediate nuclear interaction (the dash-dotted curve) accounts for an appreciable portion of the noted disagreement, and it leads to a much better description near zero energy. We consider this fact as evidence that calculations, which investigate the dependence of the ηA dynamics on the elementary amplitude $t_{\eta N}$ but disregard the interaction of the participating nucleon with the surrounding nucleons, are of little significance.

(ii) Comparison of the results obtained within the coherent approximation (30) with the four-body treatment shows the role of higher-order terms in expansion (29). As was already noted, their contribution is associated with virtual target excitations in between scatterings. As one sees, this effect is significant and increases as the energy approaches the inelastic threshold (analogous conclusions with respect to the ηd interaction are given in Ref. [22]). With increasing energy the cross section becomes similar to the one of the impulse approximation but as one sees in Fig. 3 the Argand plots remain very different.

In our opinion, the conclusions above have an important bearing on models of the η-nuclear interaction. In particular, they point to the fact that such models should not be developed as a mere repetition of the first-order π-nuclear scattering formalism.

Returning to Fig. 3 we would like to note a strong enhancement of the cross section close to zero energy as a consequence of the η^3H virtual state. The scattering length $a_{\eta^3\mathrm{H}}=(1.82+i2.75)$ fm locates the position of the pole at $E^{pole}_{\eta^3\mathrm{H}}\approx -1/(a^2_{\eta^3\mathrm{H}}\mu_{\eta^3\mathrm{H}})=(1.53+i3.59)$ MeV. The pole lies on the first nonphysical sheet ($\mathrm{Im}\sqrt{E}<0$) attached to the physical one through the two-body cut beginning at η^3H threshold [25]. The somewhat unusual behavior of the Argand plots near the inelastic threshold supposedly can be ascribed to a cusplike structure of the amplitude with a rapidly varying real part.

In order to investigate the role of the short-range nucleon-nucleon dynamics we have performed in addition a four-body calculation with a Yamaguchi parametrization of the potential v_{NN} [26] where the complicated structure of the short-range *NN* interaction is ignored. The respective result is represented by the long-dashed curve in Fig. 3. As one notes, the difference is insignificant. An obvious conclusion, which follows, is that in the low-energy region only the long-range part of the *NN* interaction comes into play, which may be described quite satisfactorily by the Yamaguchi potential. In other words, our results are not sensitive to the *NN* interaction models (which must, of course, be on-shell equivalent at low energy) as long as the momenta in question are essentially smaller than those associated with the short-range part of the *NN* force.

IV. η PHOTOPRODUCTION ON A=3 NUCLEI NEAR THRESHOLD

Turning now to η photoproduction, we treat the electromagnetic interaction as usual up to the first order in the fine structure constant. As a consequence, the photon appears only in the initial state as an incident particle. This scheme is illustrated in Fig. 4 where the electromagnetic vertex functions u^α ($\alpha=2,3$) are of first order in the γN coupling. The corresponding expression of the amplitude $Y_{11}^{(ss')}$ reads

$$Y_{11}^{(ss')}(p,k_\gamma;E)=\sum_{\alpha=2,3}\sum_{l,m}\sum_{\sigma=0,1}\int_0^\infty X^{(s\sigma)}_{\alpha 1;l1}(p,p';E)\times\Theta^{(\sigma)}_{\alpha;lm}\left(E-\frac{p'^2}{2M_\alpha}\right)U^{(\sigma s')}_{1\alpha;1m}\times(p',k_\gamma;E)\,\frac{p'^2dp'}{2\pi^2},\tag{36}$$

where the hadronic amplitudes $X_{\alpha 1}$ are defined in Sec. II [see Eq. (5)]. Here the spin coupling in the initial $\gamma 3N$ state is also uniquely determined by the spin s of the *NN* pair since the spin of the target is fixed to $S=1/2$. The effective potentials, involving the photon-induced excitation of the resonance N^*, are defined by

$$U^{(ss')}_{1\alpha;nn'}(p,k_\gamma;E)=\frac{(\Omega^{(t_\gamma)}_\alpha)_{ss'}}{2}\int_{-1}^{+1}v^{1(s)}_{d;n}(q_1,-\varepsilon_{3\mathrm{H}})\times\tau^{(s)}_d\left(-\varepsilon_{3\mathrm{H}}-\frac{3q_1^2}{4M_N}\right)u^{\alpha(ss',t_\gamma)}_{n'}(q_\alpha)d(\hat{k}_\gamma\cdot\hat{p}),\quad\alpha=2,3,\tag{37}$$

with a relative momentum at the $(3N)\to N+(NN)$ vertex $\vec{q}_1=\vec{p}+\frac{1}{3}\vec{k}_\gamma$. The form factors $u_n^{\alpha(ss',t_\gamma)}(q_\alpha)$ are associated with the absorption of a photon having isospin t_γ by a nucleon or by a nucleon pair (see Fig. 4). For the $\gamma(NN)$ and γN relative momenta q_α ($\alpha=2,3$) we use semirelativistic expressions

$$\vec{q}_2 = \vec{k}_\gamma + \frac{\omega_\gamma}{\omega_\gamma + 2M_N}\vec{p}, \quad \vec{q}_3 = \vec{k}_\gamma + \frac{\omega_\gamma}{\omega_\gamma + M_N}\vec{p}. \tag{38}$$

The spin-isospin coefficients, presented in Eq. (37) in matrix form by $\Omega_\alpha^{(t_\gamma)}$, are obtained from standard spin algebra

$$\Omega_2^{(0)} = \begin{pmatrix} 0 & 0 \\ 0 & 2\sqrt{\frac{2}{3}} \end{pmatrix}, \quad \Omega_2^{(1)} = \begin{pmatrix} 0 & \pm\sqrt{\frac{2}{3}} \\ \pm\sqrt{\frac{2}{3}} & 0 \end{pmatrix},$$

$$\Omega_3^{(0)} = \begin{pmatrix} \sqrt{6} & 0 \\ 0 & -\sqrt{\frac{2}{3}} \end{pmatrix}, \quad \Omega_3^{(1)} = \begin{pmatrix} \mp\sqrt{\frac{2}{3}} & 0 \\ 0 & \mp\sqrt{\frac{2}{3}} \end{pmatrix}, \tag{39}$$

with the upper (lower) sign referring to ^{3}He(^{3}H).

It should be noted that going from η^3H elastic scattering to η photoproduction we are faced with qualitatively new physics where large momentum transfers dominate. In particular, due to this reason, the contribution of pion exchange between the nucleons to the η production mechanism must be included in general. This fact is confirmed by several theoretical developments [27,28]. However, for reasons of principal numerical difficulties, already noted in Sec. II, we do not include pion rescattering into our calculation and make only several remarks in the conclusion.

As for the electromagnetic vertex functions u_n^α, it is easy to show that up to the first order in the γN interaction they are given by [cf. Eq. (13)]

$$u_n^{\alpha(ss',t_\gamma)}(q_\alpha) = \int_0^\infty \widetilde{V}_{\alpha;dN^*}^{(s,t_\gamma)}(q_\alpha, q')\ \tau_{N^*}\left(B_\alpha - \frac{q'^2}{2\mu_{N^*}^\alpha}\right) v_{N^*;n}^{\alpha(s')} \times (q', B_\alpha)\frac{q'^2 dq'}{2\pi^2}, \quad \alpha = 2, 3, \tag{40}$$

where the effective potentials $\widetilde{V}_{\alpha;dN^*}^{(s,t_\gamma)}$ are determined analogous to the hadronic potentials $V_{\alpha;dN^*}$ [4] but with an incident η replaced by a photon

$$\widetilde{V}_{2;dN^*}^{(s,t_\gamma)}(q_2, q') = -\frac{1}{\sqrt{2}}\int_{-1}^{+1} \frac{g_d^{(s)}\left(\left|\vec{q}' + \frac{1}{2}\vec{q}_2\right|\right)\tilde{g}_{N^*}^{(t_\gamma)}\left(\left|\vec{q}_2 + \frac{\omega_\gamma}{\omega_\gamma + M_N}\vec{q}'\right|, \omega_{N^*}\right)}{\varepsilon_{^3\mathrm{H}} + \frac{3}{4M_N}\left(\vec{p} + \frac{1}{3}\vec{k}_\gamma\right)^2 + \frac{1}{M_N}\left(\vec{q}' + \frac{1}{2}\vec{q}_2\right)^2} d(\hat{q}\cdot\hat{q}'), \tag{41}$$

$$\widetilde{V}_{3;dN^*}^{(s,t_\gamma)}(q_3, q') = -\frac{g_d^{(s)}(q')\tilde{g}_{N^*}^{(t_\gamma)}(q_3, \omega_{N^*})}{\varepsilon_{^3\mathrm{H}} + \frac{3}{4M_N}\left(\vec{p} + \frac{1}{3}\vec{k}_\gamma\right)^2 + \frac{1}{M_N}q'^2}, \tag{42}$$

where $\tilde{g}_{N^*}^{(t_\gamma)}(k_{\gamma N}, \omega_{N^*})$ denotes the $\gamma N \to N^*$ vertex functions depending on the γN c.m. momentum $k_{\gamma N}$ and the invariant ηN energy ω_{N^*}. The denominators in expressions (41) and (42) are obtained by taking into account the on-shell conditions in the initial γ^3H state, i.e., $E = -\varepsilon_{^3\mathrm{H}} + \omega_\gamma - m_\eta + k_\gamma^2/2M_{^3\mathrm{H}}$ as well as the dependence of the momenta $\vec{q}_2$ and $\vec{q}_3$ on $\vec{k}_\gamma$ and $\vec{p}$ given by Eq. (38). One readily sees that the singularities on the real q' axis are never reached in $\widetilde{V}_{\alpha;ij}$.

In the actual calculation, we treat the vertices $\tilde{g}_{N^*}^{(t_\gamma)}(k, \omega_{N^*})$ independent of the momentum k and parametrize their behavior in the following form

$$\tilde{g}_{N^*}^{(1)}(k, \omega_{N^*}) = \begin{cases} \frac{e}{\sqrt{4\pi}}\sum_{n=0}^{4} a_n\left(\frac{k_\pi}{m_\pi}\right)^n, & \omega_{N^*} > M_N + m_\pi, \\ \tilde{g}_{N^*}^{(1)}(k, \omega_{N^*})|_{\omega_{N^*} = M_N + m_\pi} & \text{else}, \end{cases} \tag{43}$$

$$\tilde{g}_{N^*}^{(0)}(k, \omega_{N^*}) = 0.1\ \tilde{g}_{N^*}^{(1)}(k, \omega_{N^*}),$$

where k_π is the on-shell pion momentum in the πN c.m. frame corresponding to the total energy ω_{N^*}. The isospin separation of the $S_{11}(1535)$ photoexcitation amplitude is chosen such that the relation

$$\frac{\sigma(\gamma p \to \eta p)}{\sigma(\gamma n \to \eta n)} = 0.67 \tag{44}$$

is reproduced in accordance with the experimental results for quasifree η photoproduction on light nuclei [29,30]. The coefficients in Eq. (43),

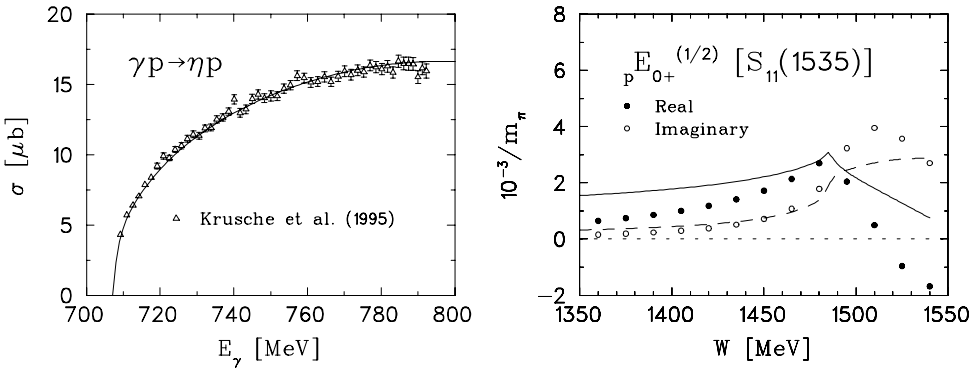

FIG. 5. Left panel: the $\gamma p \to \eta p$ total cross section compared with the data of Ref. [31]. Right panel: the ${}_pE_{0^+}^{(1/2)}$ multipole of $\gamma p \to \pi p$ generated by the photoexcitation of the $S_{11}(1535)$ resonance. Solid curve—real part, dashed curve—imaginary part. Open and filled circles represent the results of the MAID parametrization [32].

$$a_0 = 5.007 \times 10^{-1}, \quad a_1 = -1.750 \times 10^{-2},$$

$$a_2 = 0.926 \times 10^{-1}, \quad a_3 = 2.052 \times 10^{-3},$$

$$a_4 = -6.408 \times 10^{-3}, \tag{45}$$

were obtained by fitting the $\gamma p \to \eta p$ data [31] as shown in Fig. 5. In the same figure we also compare our calculation of the $\gamma p \to S_{11}(1535) \to \pi p$ amplitude ${}_pE_{0^+}^{(1/2)}$ with the results of the MAID parametrization [32]. For definiteness, we present here the elementary photoproduction amplitude for $\gamma p \to \pi p$,

$$t_\lambda = {}_pE_{0^+}^{(1/2)}(\vec{\sigma} \cdot \vec{\varepsilon}_\lambda),$$

$$\text{with } {}_pE_{0^+}^{(1/2)} = \left[\tilde{g}_{N^*}^{(0)}(k_\gamma, \omega_{N^*}) + \tilde{g}_{N^*}^{(1)}(k_\gamma, \omega_{N^*})\right] \times \tau_{N^*}(\omega_{N^*} - M_N - m_\eta) g_{N^*}^{(\eta)}(k_\eta). \tag{46}$$

The c.m. differential cross section then reads

$$\frac{d\sigma}{d\Omega}(\gamma p \to \eta p) = \frac{k_\eta}{k_\gamma} \frac{2\omega_\eta E_{N_i} E_{N_f}}{(4\pi\omega_{N^*})^2} |{}_pE_{0^+}^{(1/2)}|^2, \tag{47}$$

with ω_η and $E_{N_{i(f)}}$ denoting the energies of the η meson and the initial (final) nucleon, respectively.

Before completing the formal part, we recall once more that all the expressions above relate only to the *s* wave. With increasing energy, higher partial waves, where however no significant interaction is expected, are needed to fill the available phase space. To take into account their contribution we use here the standard prescription

$$Y = Y_{PW} + [\, Y - Y_{PW}]_{L=0}, \tag{48}$$

where Y_{PW} is the plane-wave approximation to the production amplitude. Assuming that the hadronic interaction in the higher partial waves is insignificant, the difference in the parenthesis is reduced to *s* waves only. The amplitude $Y_{L=0}$ is given by Eq. (36). The diagrammatic representation of the amplitude Y_{PW} is presented in Fig. 6. The corresponding analytic expression is easily obtained and need not be presented here. We note only that each term in the sum is represented by a six-dimensional integral, which were calculated numerically without any approximation.

The reaction matrix element for the transition between the nuclear states with spin 1/2 is related to amplitude (48) by the Wigner-Eckart formula

$$\left\langle \frac{1}{2} M_f \middle| T_\lambda \middle| \frac{1}{2} M_i \right\rangle = \frac{1}{\sqrt{2}} \left(\frac{1}{2} M_i \; \lambda \middle| \frac{1}{2} M_f \right) \sum_{ss'=0,1} Y^{(ss')}. \tag{49}$$

For the unpolarized c.m. cross section, we obtain

$$\frac{d\sigma}{d\Omega}(\gamma A \to \eta A) = \frac{k_\eta}{k_\gamma} \frac{2\omega_\eta E_{A_i} E_{A_f}}{(4\pi W)^2} \frac{1}{6} \left| \sum_{ss'=0,1} Y^{(ss')}(\vec{k}_\gamma, \vec{k}_\eta) \right|^2, \tag{50}$$

with $E_{A_{i(f)}}$ being the total target energy in the initial (final) state.

Our predictions for total as well as differential cross sections are shown in Fig. 7. First we note an approximate equality

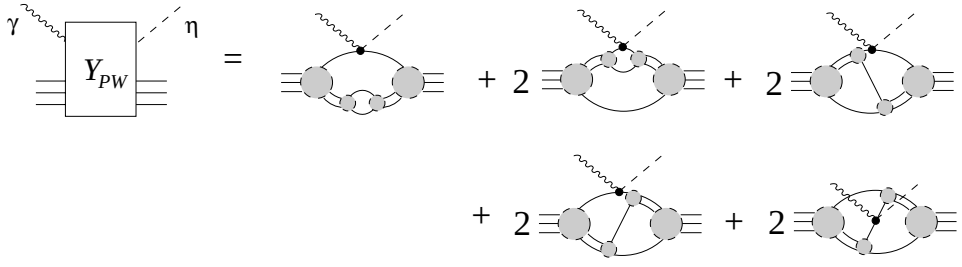

FIG. 6. Schematic representation of the plane-wave term in the η photoproduction amplitude (48) related to our model of the target wave function (17) and (18). The factor 2 stems from the identity of the nucleons.

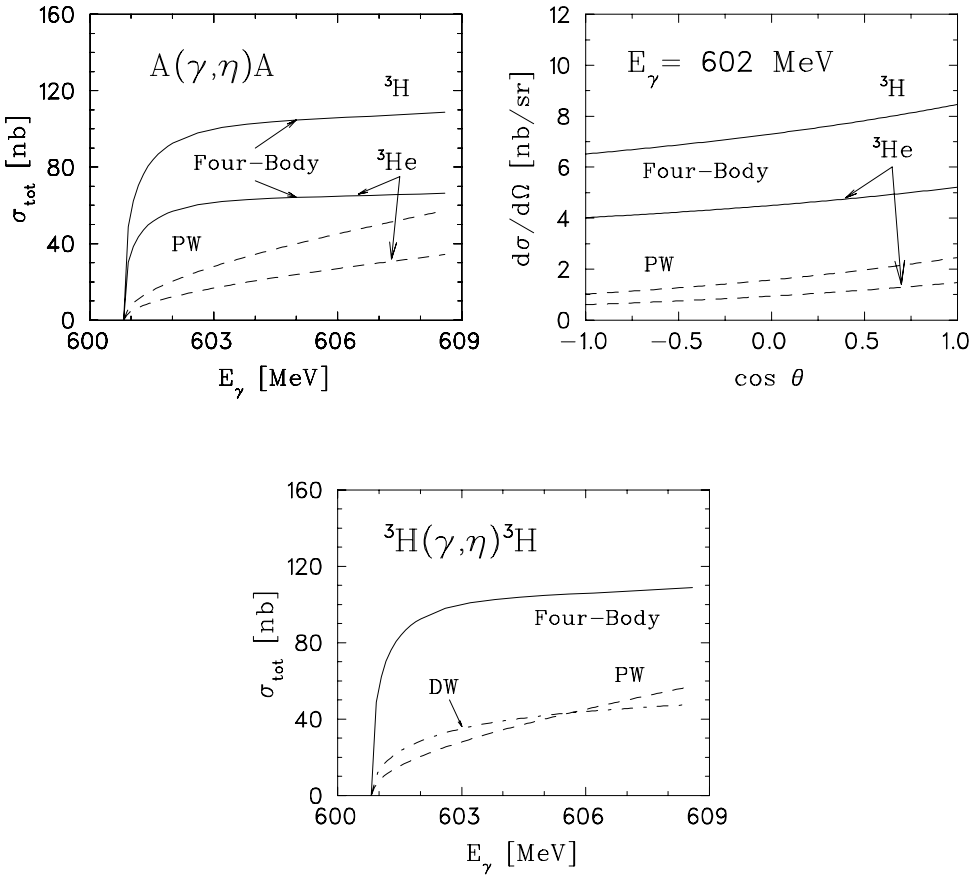

FIG. 7. Upper panels: total and differential cross section for η photoproduction on ^{3}He and ^{3}H calculated within the four-body scattering model for the final $\eta\,3N$ system compared to the results of the plane-wave calculation (the dashed curves on both panels). In the lower panel the FSI effects provided by the distorted wave (DW) approach with the optical potential (32) (dash-dotted curve) are compared with those given by the four-body calculation and the plane-wave approximation (PW).

$$\frac{\sigma(\gamma n \to \eta n)}{\sigma(\gamma p \to \eta p)} \approx \frac{\sigma(\gamma\,^3\mathrm{He} \to \eta\,^3\mathrm{He})}{\sigma(\gamma\,^3\mathrm{H} \to \eta\,^3\mathrm{H})} \approx 0.6. \qquad (51)$$

As was already explained in Refs. [10,33] this result is a consequence of the spin-flip nature of the η photoproduction amplitude t_λ (46). Approximating the spatial part of the target wave function (17) by only the principal, totally symmetric s state it is easy to see that the η meson can only be produced on the neutron in ^{3}He and on the proton in ^{3}H. The remaining two nucleons, coupled to a total spin $s=0$, do not participate due to the Pauli principle. The η-rescattering effects, being spin independent do not distort this relation. A small deviation from relation (44) is simply due to the presence of the state with mixed permutation symmetry.

As expected, the final state interaction leads to a rather pronounced enhancement of the plane-wave result, especially very close to the production threshold. The cross section reaches very fast its characteristic value and has a form of a flat plateau. The angular distribution of η mesons in both reactions is shown in the upper right panel of Fig. 7. Within our model only the angular-independent s-wave part of the $\eta\,3N$ wave function undergoes distortion due to the FSI. As a consequence, the differential cross section is much more isotropic as compared with the plane-wave calculation.

Comparing our results for $^3\mathrm{He}(\gamma,\eta)^3\mathrm{He}$ reaction with those of Ref. [10] obtained within the FRA, we observe rather well agreement in magnitude of the total cross sections close to the threshold (we take for comparison the results of Refs. [10] corresponding to the model IIIa for the ηN interaction). However we think, this fact has no physical significance, since there are principal differences in the models. First, we would like to note a disagreement concerning the nature of the final state interaction. Namely, as explained in Ref. [10] the strong effect of FSI, found by the authors, is due to the s-wave $\eta\,3N$ resonance, located near zero kinetic energy [34]. In our case it is a consequence of the virtual state, as was already discussed in Ref. [4]. We do not find any evidence for the resonance behavior of the η^3H amplitude (see, e.g., the Argand plots in Fig. 3). Furthermore, our calculation does not exhibit a strong slope in the cross section caused by a cusp at the inelastic threshold, which was found to be very pronounced in Ref. [10].

In the lower panel of Fig. 7, we also depict the total cross section for the reaction on ^{3}H where the final state is distorted by the first-order optical potential [the approximation denoted as (distorted wave) DW]. The corresponding photoproduction amplitude is given by [cf. Eq. (33)]

$$Y(\vec{k}_\eta, \vec{k}_\gamma; E) = Y_{PW}(\vec{k}_\eta, \vec{k}_\gamma; E) + \frac{2}{3}\,\frac{\mu_{\eta^3\mathrm{H}}}{\pi^2} \times \int_0^\infty \frac{T(k_\eta, p; E)[Y_{PW}(\vec{p}, \vec{k}_\gamma; E)]_{L=0}}{k_\eta^2 - p^2 + i\varepsilon} p^2 dp, \tag{52}$$

where the T matrix for the η^3H scattering $T(k_\eta, p; E)$ was calculated with the potential (32). As one readily notes, the DW approach visibly underestimates the strong FSI effect of the four-body theory.

A comparison of the DW calculation for the reaction $^3\mathrm{He}(\gamma, \eta)^3\mathrm{He}$ with the full model has also been done in Ref. [10]. In particular, the authors have noted a very large difference between the cross sections obtained within FRA and DW approaches. At the energy E_γ=605 MeV the DW results reported in Ref. [10] underpredict those of the FRA model by about a factor of 20. The reason of this disagreement is a very strong suppression of the DW cross section in the near-threshold region. In contrast to this conclusion, our calculation predicts a typical *s*-wave energy dependence of the cross section for the coherent reaction of the form

$$\sigma \sim \sqrt{E_\gamma - E_\gamma^{th}}, \tag{53}$$

with E_γ^{th} denoting the threshold energy. This form is slightly distorted by the η-nuclear optical potential which tends to increase the cross section value close to the threshold. As a consequence the difference between the DW result and the full four-body calculation turns out to be not so impressive as in Ref. [10].

V. CONCLUSION

In the present paper we have investigated elastic scattering and photoproduction of η mesons on three-body nuclei near threshold. The possibility of having the exact solution at hand permits us to investigate unambiguously the corrections to the lowest-order optical potential which are usually neglected within the "standard" optical model approach. According to the results presented above, we would like to draw the following conclusions.

(i) The contributions beyond the impulse approximation turn out to be very important. It is reasonable to assume that the origin of this fact lies in the resonance nature of the ηN amplitude giving rise to large corrections caused by the binding of the nucleons. One may expect that this effect is even stronger in heavier nuclei.

(ii) The influence of virtual target excitations between successive scatterings is also rather important. Although the three- and four-body thresholds are relatively far from the $3N$ binding energy, neglect of the excited states makes the result very different from the exact one. In other words, the contributions of virtual three- and four-body states are also quite important below the corresponding unitary cuts.

(iii) Since in the energy region considered here the incident energy of the η-meson remains small, i.e., its wavelength is large compared to the characteristic internuclear distance, the results for the η^3H scattering are not visibly sensitive to the details of the short-range *NN* dynamics. This conclusion is confirmed straightforwardly comparing the results of the PEST potential [14] with those given by the simplest Yamaguchi form of the *NN* interaction.

(iv) Close to the threshold, the final state interaction enhances the η yields appreciably, which was already noted in a variety of studies of η production on lightest nuclei with different entry channels [35–37]. The angular distribution shows pronounced isotropy, associated with the *s*-wave dominance of FSI.

In conclusion, we would like to note once more the possible importance of pion exchange in the η photoproduction on nuclei. One can expect this since the suppression due to the strong momentum transfer which is presumably important for low-energy $\eta 3N$ scattering appears not to be effective here. Furthermore, as was already noted, due to the spin-flip nature of the η photoproduction mechanism, only $\approx 1/3$ of the nucleons are involved in the process. This may further enhance the importance of the π-exchange contribution where the nonvanishing non-spin-flip part gives rise to a coherent enhancement of the reaction strength. A good case in point is the pion production via $\Delta(1232)$ excitation (the spin-independent part dominates) with subsequent rescattering into η through the excitation of $S_{11}(1535)$ (the spin-flip part is negligible) on the next nucleon. On the other hand, we suppose that due to the short-range nature of the pion-rescattering mechanism its contribution does not influence the strong energy dependence of the cross section discussed above but its magnitude can be visibly affected.

ACKNOWLEDGMENT

The work was supported by the Deutsche Forschungsgemeinschaft (SFB 443).

[1] T. Ueda, Phys. Rev. Lett. **66**, 297 (1991); Phys. Lett. B **291**, 228 (1992).
[2] C. Wilkin, Phys. Rev. C **47**, R938 (1993).
[3] S. Wycech, A. M. Green, and J. A. Niskanen, Phys. Rev. C **52**, 544 (1995).
[4] A. Fix and H. Arenhövel, Phys. Rev. C **66**, 024002 (2002).
[5] M. Ericson and T. E. O. Ericson, Ann. Phys. (N.Y.) **36**, 323 (1966).
[6] I. R. Afnan and A. T. Stelbovics, Phys. Rev. C **23**, 845 (1981).
[7] H. Garcilazo, Phys. Rev. C **25**, 2596 (1982).
[8] J. Kuros, H. Witala, W. Glöckle, J. Golak, D. Hüber, and H. Kamada, Phys. Rev. C **56**, 654 (1997).
[9] M. Pfeiffer, Ph.D. thesis, University of Giessen, Giessen, 2002.
[10] N. V. Shevchenko *et al.*, Nucl. Phys. **A699**, 165 (2002).
[11] S. A. Sofianos, N. J. McGurk, and H. Fiedeldey, Nucl. Phys.

A318, 295 (1979).
[12] A. C. Fonseca, *Proceedings of the Eighth Autumn School on Models and Methods in Few-Body Physics*, Lisboa, 1986, edited by L. S. Ferreira, A. C. Fonseca, and L. Streit [Lect. Notes Phys. **273**, 161 (1986)].
[13] There are separable expansion methods, which seem to be capable of approximating the three-body off-shell scattering amplitudes also at positive energies (see, e.g., A. C. Fonseca, H. Haberzettl, and E. Cravo, Report No. BONN-HE-82). But they require far more numerical efforts and were not adopted here.
[14] H. Zankel, W. Plessas, and J. Haidenbauer, Phys. Rev. C **28**, 538 (1983).
[15] Q. Haider and L. C. Liu, Phys. Rev. C **66**, 045208 (2002).
[16] C. Bennhold and H. Tanabe, Nucl. Phys. **A530**, 625 (1991).
[17] R. A. Arndt, J. M. Ford, and L. D. Roper, Phys. Rev. D **32**, 1085 (1985).
[18] M. Batinić, I. Šlaus, A. Švarc, and B.M. K. Nefkens, Phys. Rev. C **51**, 2310 (1995).
[19] M. L. Goldberger and K. M. Watson, *Collision Theory* (Wiley, New York, 1964).
[20] A. K. Kerman, H. McManus, and R. M. Thaler, Ann. Phys. (N.Y.) **8**, 551 (1959).
[21] R. Aaron, R. D. Amado, and Y. Y. Yam, Phys. Rev. **136**, B650 (1964).
[22] S. Wycech and A. M. Green, Phys. Rev. C **64**, 045206 (2001).
[23] H. P. Noyes, Phys. Rev. Lett. **15**, 538 (1965); K. L. Kowalski, *ibid.* **15**, 798 (1965).
[24] R. S. Hayano, S. Hirenzaki, and A. Gillitzer, Eur. Phys. J. A **6**, 99 (1999).
[25] More exactly, there are two poles which are placed symmetrically about the real energy axis.
[26] Y. Yamaguchi, Phys. Rev. **95**, 1628 (1954).
[27] L. C. Liu, Phys. Lett. B **288**, 288 (1992).
[28] F. Ritz and H. Arenhövel, Phys. Rev. C **64**, 034005 (2001).
[29] P. Hoffmann-Rothe *et al.*, Phys. Rev. Lett. **78**, 4697 (1997).
[30] V. Hejny *et al.*, Eur. Phys. J. A **6**, 83 (1999).
[31] B. Krusche *et al.*, Phys. Rev. Lett. **74**, 3736 (1995).
[32] D. Drechsel, O. Hanstein, S. S. Kamalov, and L. Tiator, Nucl. Phys. **A645**, 145 (1999).
[33] L. Tiator, C. Bennhold, and S. S. Kamalov, Nucl. Phys. **A580**, 455 (1994).
[34] V. B. Belyaev, S. A. Rakityansky, S. A. Sofianos, M. Braun, and W. Sandhas, Few-Body Syst., Suppl. **8**, 309 (1995); S. A. Rakityansky, S. A. Sofianos, M. Braun, V. B. Belyaev, and W. Sandhas, Phys. Rev. C **53**, R2043 (1996).
[35] B. Mayer *et al.*, Phys. Rev. C **53**, 2068 (1996).
[36] H. Calen *et al.*, Phys. Rev. Lett. **79**, 2642 (1997).
[37] V. Hejny *et al.*, Eur. Phys. J. A **13**, 493 (2002).